scientific reports

OPEN

Development of a quartz-based geothermometer for biogenic chert

Haruka Tanaka[1], Sharav Davaanyam[2], Bayart Nadmid[1] & Kazuhiro Tsukada[3✉]

In the accretionary complexes of areas where erosion is inactive, only biogenic chert is sometimes exposed and estimating diagenetic/metamorphic temperature in such areas is nearly impossible. We investigated the correlation of quartz crystallinity (CI), grain size (GS), and diagenetic/metamorphic temperature (PT) of biogenic chert and developed a quartz-based geothermometer to contribute to the advancement of tectonics in such regions. Sediments of microbial remains comprising amorphous silica can transform into biogenic chert/metachert during diagenesis/metamorphism through an increase in CI and GS. However, the relationship between CI, GS, and PT remains underexplored. By examining Paleozoic–Mesozoic biogenic chert/metachert from four regions of East Asia, we identified a systematic relationship between CI, GS, and PT. In cryptocrystalline chert (GS ≤ 1.94 μm), CI and GS exhibit a strong logarithmic relationship, whereas in crystalline chert, CI approaches its upper limit and GS widely varies. These relationships are consistent across four studied regions, irrespective of their geological age and location. CI and GS increase with increasing PT, with a positive linear relationship between CI and PT and a logarithmic relationship between GS and PT. CI and GS strongly correlate with PT (R > 0.929), making them reliable geothermometers for estimating diagenetic/metamorphic temperature.

A geothermometer is used for measuring paleotemperature (PT) experienced by rocks. Some geothermometer approaches rely on the relationship between PT and phase equilibrium or mineral reaction rates and others use the correlation between PT and mineral crystallinity. Minerals in pelitic rocks are generally used as geothermometers for sedimentary rocks. However, in regions such as within a continent, where erosion is inactive and alluvial sediments predominantly cover the rocks. Therefore, in such regions, it is challenging to estimate the PT of the geologic units and understand the detailed tectonic history, especially in accretionary complexes formed by the subduction of an earlier oceanic plate. Biogenic chert, primarily composed of quartz, often forms exposed ridges due to its resistance to weathering, even in regions where pelitic rocks are absent (Fig. 1). Therefore, if the PT of biogenic chert is estimated, tectonics research in such regions may be greatly advanced.

Sediments composed of siliceous microbial remains, such as those of radiolarians, transform into biogenic chert and metachert through diagenesis and metamorphism, respectively, wherein amorphous silica is converted into quartz, often through the opal-CT phase[1,2,4]. Quartz crystallinity (CI)[3] and grain size (GS) are believed to increase with increasing PT[4–6]. Numerous studies on the transformation of amorphous silica into quartz have been conducted[4]. It has been confirmed that higher temperatures lead to a higher conversion rate of amorphous silica into quartz, and the activation energy for this reaction has been calculated[7–11]. These results have been used to understand the mechanisms in the early stage of the diagenesis of silica deposits[7,11–15].

However, the relationship between quartz CI and GS after the early stage of diagenesis as well as their correlation with PT remain unclear. For the radiolarian chert obtained from the Jurassic accretionary complex of the Tanba belt, Japan, it has been suggested that quartz CI and GS show a logarithmic relationship—CI and GS increasing as PT rises—based on the color index of co-existing conodont fossils[16]. Although the cited study provides an overview of the relationship between CI, GS, and PT, its accuracy seems insufficient. Moreover, the CI of radiolarian chert and metachert obtained from the Khangai–Daur belt, a Carboniferous accretionary complex in Mongolia, was reported to increase sharply with increasing GS. Even after CI has almost reached its maximum (8–10), GS continues to increase[17]. However, the detailed relationship between CI and GS as well as PT conditions experienced by the rocks remain unspecified. Clarifying the correlation between CI, GS, and PT can provide valuable insights into the tectonics of orogenic belts, especially in regions where other rock types are scarce.

This study investigated the relationship between the CI, GS, and PT of biogenic chert and metachert obtained from East Asia, specifically from accretionary complexes in Japan (Chubu province and Ashimidani area)[18],

[1]Graduate School of Environmental Studies, Nagoya University, Nagoya 464-8601, Japan. [2]Institute of Geology, Mongolian Academy of Science, Ulaanbaatar 18080, Mongolia. [3]Nagoya University Museum, Nagoya 464-8601, Japan. ✉email: tsukada@num.nagoya-u.ac.jp
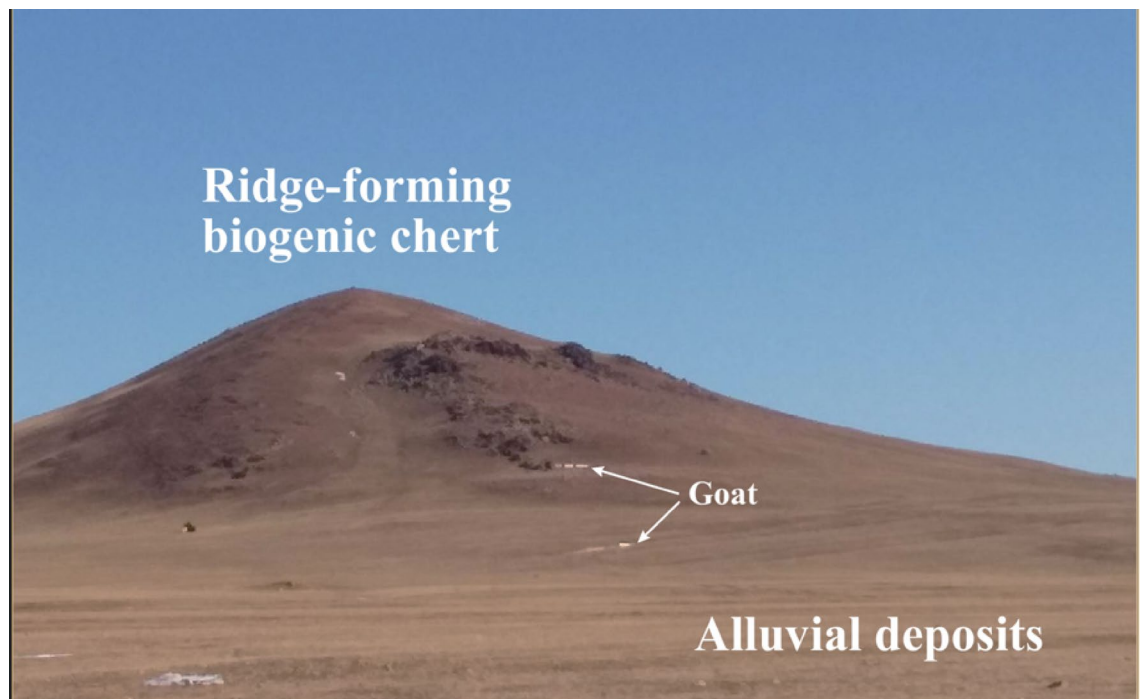
Fig. 1. Ridge-forming Silurian–Devonian biogenic chert in the Carboniferous accretionary complex of the Khangai–Daur belt, Mongolia.

Russia (Anyui area)[19,20], and Mongolia (Ulaanbaatar area)[21,22] (Figs. 1 and 2). In addition, the relationship between the CI or GS and PT of cryptocrystalline chert was discussed compared with the PT for mudstone, which conformably overlies the cryptocrystalline chert, to develop a new geothermometer. CI, GS, and PT were determined using X-ray diffraction (XRD), scanning electron microscopy (SEM)/optical microscopy, and a Raman spectra of carbonaceous material (RSCM) geothermometer, respectively[3,16,24]. The results from the CI, GS, and PT measurements of each sample were analyzed using linear regression analysis with the least squares method to determine the relationships between the variables.

Samples analyzed
Samples of biogenic chert and metachert
A total of 112 samples from four regions were analyzed (Fig. 2; Table 1): 64 samples from Japan (Mino and Ryoke belts in Chubu province and the Tanba belt in the Ashimidani area)[18], 14 from Russia (Samarka terrane and the Anyui metamorphic complex in the Anyui area)[19,20], and 34 from Mongolia (Ulaanbaatar terrane at Ulaanbaatar area)[21,22]. These samples were selected based on their composition, and only those without significant secondary alteration or microquartz veins were analyzed.

Microfossils from the Middle Triassic to Middle Jurassic, including those of radiolarians and conodonts were recovered from chert in the Mino belt of the Jurassic accretionary complex of the study area[25–28]. The Ryoke belt is generally considered the metamorphosed facies of the Mino belt[18]. Microfossils of Permian radiolarians and conodonts have been found in chert of the Tanba belt, Ashimidani area, Japan[29]. The Samarka terrane and Anyui metamorphic complex, located ~ 250 km northeast of Khabarovsk, are the Jurassic–Cretaceous accretionary complex and its metamorphosed form, respectively[20]. Middle Triassic to Middle Jurassic radiolarians and conodonts were recovered from chert obtained from the Samarka terrane[20]. The Carboniferous accretionary complex of the Ulaanbaatar terrane, lying within the Eurasian continent, contains radiolarian chert from the Upper Silurian to the Upper Devonian[22].

Samples from the Ryoke belt and Anyui metamorphic complex underwent contact metamorphism owing to Cretaceous igneous activity[18,20]. Some samples obtained from the Samarka and Ulaanbaatar terranes were also metamorphosed[17,21].

All samples—composed mostly of quartz—were obtained from well-bedded chert or metachert outcrops (Fig. 3a). In the outcrops, chert or metachert layers with a thickness of several centimeters alternated with thin muddy films with a thickness of < 5 mm (Fig. 3a). Only the central part of the chert layer was examined as the part in contact with the thin muddy films may have undergone alteration[4]. As per microscopy results, the chert samples from the Mino and Tanba belts and the Samarka and Ulaanbaatar terranes were composed mainly of cryptocrystalline quartz. Individual crystals were difficult to identify at 40 × magnification and contained well-preserved or poorly preserved radiolarian tests (Fig. 3b; Table 1). Chert samples whose biogenic origin could not be verified, such as those lacking fossil remains, were not used in this study. The metachert samples from the Ryoke belt, the Samarka and Ulaanbaatar terranes, and the Anyui metamorphic complex comprised crystalline quartz (Fig. 3c and d; Table 1). Although no distinct fossil remains were visible in the metachert
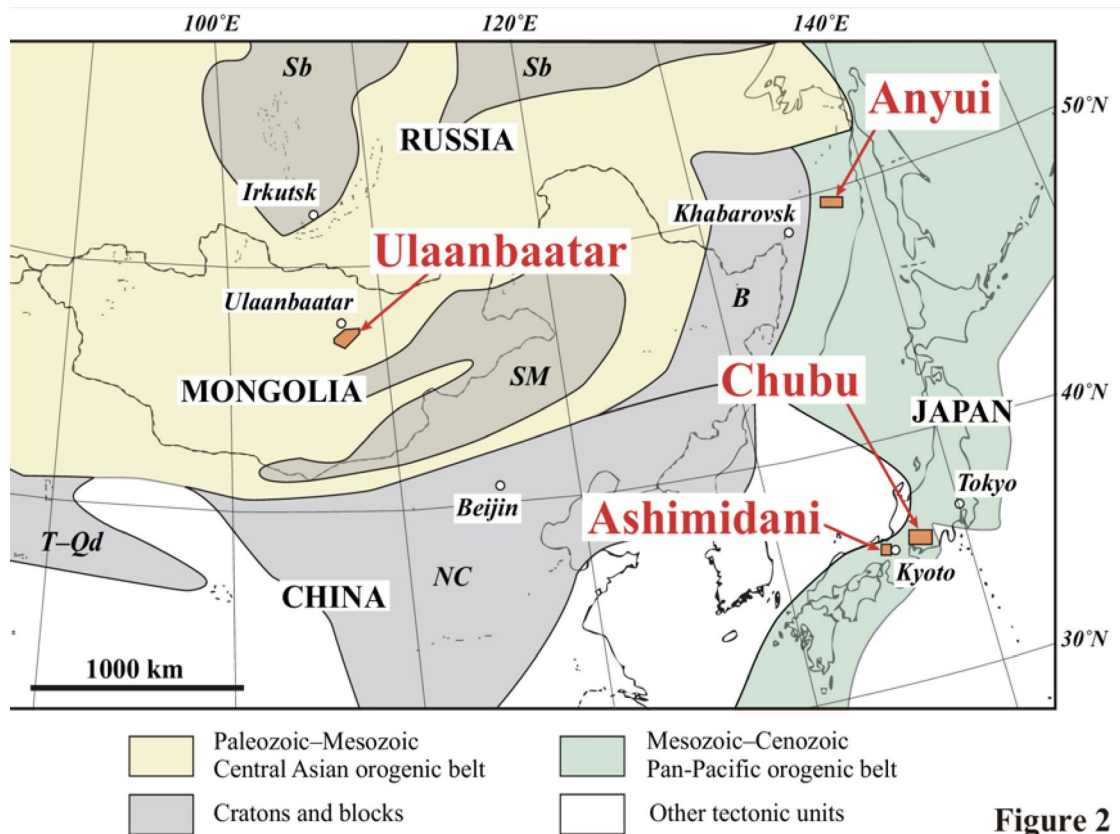
Fig. 2. Index map of the study areas. Modified from Umeda et al. (2022)[23]. Sb: Siberian craton, NC: North China block, T–Qd: Tarim–Qaidam block, SM: South Mongolian block, B: Bureya block.

samples, a biogenic origin could be inferred as the origin field closely resembled that of radiolarian chert—well-bedded field with several-centimeter-thick layers and thin muddy interbeds. Approximately 54% of the analyzed samples consisted of cryptocrystalline quartz containing numerous radiolarian tests and 46% comprised crystalline quartz. Microscopic observations of thin sections in different directions of each sample confirmed that the quartz grains of all samples showed no particular anisotropy. Crystallinity index (CI) was determined based on XRD and GS was measured using SEM or optical microscopy.

Samples of the mudstone
Nine samples were collected from mudstone layers present near the chert exposed in the Mino and Tanba belts, Japan, for PT measurement using an RSCM geothermometer[24]. The mudstone outcrops were located approximately 5–800 m from the chert outcrops and stratigraphically present above them, following oceanic plate stratigraphy (Fig. 3 e and f)[30–33]. The mudstone samples were black to dark gray, mostly undeformed, well laminated, or alternating with sandstone (Fig. 3f). Microscopic examination of the samples showed no signs of shearing. The RSCM geothermometer was used to estimate the PT of the mudstone samples, which were obtained from nearby outcrops, to compare it with that of the chert samples.

Analytical methods
CI of the biogenic chert and metachert samples
The CI of all samples was measured using XRD (MultiFlex, Rigaku Corporation), installed at the Nagoya University Museum by following the method reported by Murata and Norman[3]. The samples were crushed and sieved to 75 μm. Then, SEM observation confirmed that most particles were in the range of 1–20 μm. The powdered samples were mounted in a glass holder for the measurement. Device background settings of XRD were as follows: X-ray: Ni–filtered copper radiation, scanning range: $2\theta = 65°$–70°, scanning speed: 1°/minute, voltage: 40 kV, current: 4 mA, and divergence slit: 1°.

The CI of the samples was calculated from the intensity of the (212) peak at $2\theta = 67.74°$ of the samples using the following equation[3]:

CI = 10 F a / b.

The values "a" and "b" are shown in Fig. 4. Herein, euhedral quartz obtained from the Minas Gerais, Brazil was used as the standard sample to calculate the F value. The values of "a" and "b" determined from the analysis of the standard quartz sample were substituted into the above formula and found the F value as $CI = 10^3$. The analysis process of this research was divided into 15 sessions, and the F value was calculated each time (1.33–1.57).

Area	Geologic unit	Sample No	Latitude	Longitude	CI	GS	Classification	*PT*
Chubu, Japan	Ryoke	2	35°16′33.76"N	137° 4′52.70"E	7.84	46.1	Cst	
	Ryoke	4	35°21′5.41"N	137° 8′15.29"E	9.84	7.46	Cst	
	Ryoke	5	35°23′3.02"N	137° 9′20.47"E	9.44	18.4	Cst	
	Ryoke	6	35°23′3.02"N	137° 9′20.47"E	9.05	14.8	Cst	
	Mino	7	35°24′25.58"N	137° 7′32.78"E	5.10	0.900	Cpt	
	Mino	8	35°24′40.43"N	137° 0′6.07"E	3.17	0.499	Cpt	
	Mino	10	35°24′4.66"N	136°57′40.32"E	2.58	0.451	Cpt	214
	Mino	11	35°24′4.66"N	136°57′40.32"E	3.94	0.370	Cpt	
	Mino	12	35°24′4.66"N	136°57′40.32"E	2.53	0.341	Cpt	
	Mino-Ryoke	16	35°20′50.45"N	137° 0′53.77"E	7.94	1.94	Cpt	
	Mino-Ryoke	20	35°18′27.49"N	137° 6′21.23"E	7.45	2.55	Cpt	
	Ryoke	21	35°16′37.44"N	137° 7′21.36"E	8.62	46.2	Cst	
	Ryoke	23	35°18′55.04"N	137° 4′39.53"E	9.20	5.88	Cst	
	Mino-Ryoke	25	35°19′10.60"N	137° 5′19.22"E	9.12	1.82	Cpt	320
	Ryoke	28	35°19′9.26"N	137° 0′7.44"E	8.68	69.6	Cst	
	Ryoke	31	35°20′54.68"N	137° 1′14.27"E	8.13	8.22	Cst	
	Ryoke	32	35°15′54.98"N	137° 3′16.76"E	8.76	47.8	Cst	
	Ryoke	38	35°28′28.52"N	137°11′35.04"E	9.61	22.7	Cst	
	Mino	40	35°30′12.66"N	137° 0′51.49"E	3.35	0.341	Cpt	
	Mino	43	35°40′43.35"N	137° 1′4.29"E	2.93	0.397	Cpt	
	Mino	44	35°34′47.17"N	137° 0′8.44"E	2.23	0.306	Cpt	202
	Mino	47	35°32′25.16"N	137° 3′26.46"E	1.99	0.486	Cpt	
	Mino	48	35°33′17.82"N	137° 3′12.98"E	1.98	0.339	Cpt	
	Mino	49	35°33′57.04"N	137° 4′8.09"E	3.67	0.455	Cpt	
	Mino	50	35°35′23.00"N	137° 6′46.37"E	6.60	0.668	Cpt	
	Ryoke	54	35° 7′35.32"N	137°34′48.13"E	9.80	506	Cst	
	Ryoke	56	35° 6′2.93"N	137°33′37.44"E	9.93	577	Cst	
	Ryoke	62	34°55′52.19"N	137°16′37.44"E	8.54	202	Cst	
	Ryoke	65	34°55′24.41"N	137°20′42.84"E	9.53	218	Cst	
	Ryoke	67	34°56′9.72"N	137°21′32.80"E	8.89	58.5	Cst	
	Ryoke	68	34°55′42.01"N	137°20′53.94"E	8.80	125	Cst	
	Ryoke	75	34°51′10.14"N	137° 8′38.81"E	8.78	333	Cst	
	Ryoke	76	34°51′13.01"N	137° 8′44.32"E	7.00	397	Cst	
	Ryoke	78	34°48′40.40"N	137° 6′47.24"E	8.40	201	Cst	
	Ryoke	79	35°48′32.36"N	138° 0′24.34"E	7.25	137	Cst	
	Ryoke	84	35°41′57.22"N	137°59′31.73"E	8.62	367	Cst	
	Ryoke	87	35°59′23.73"N	137°59′23.10"E	7.85	14.2	Cst	
	Mino	93	35°55′19.10"N	137°46′11.83"E	6.77	1.62	Cpt	296
	Mino-Ryoke	94	35°57′18.63"N	137°48′33.22"E	8.30	7.37	Cst	
	Mino-Ryoke	95	35°57′18.63"N	137°48′33.22"E	8.79	2.86	Cst	
	Mino	96	35°58′45.71"N	137°49′8.83"E	6.23	1.10	Cpt	290
	Mino	97	35°58′45.71"N	137°49′8.83"E	7.73	1.15	Cpt	
	Mino	105	35°50′26.71"N	137°39′22.01"E	6.60	1.99	Cpt	
	Mino	106	35°52′39.91"N	137°41′52.43"E	4.72	0.689	Cpt	255
	Mino	108	35°56′4.19"N	137°36′39.43"E	4.53	0.587	Cpt	
	Mino	109	35°56′22.10"N	137°35′10.67"E	2.03	0.439	Cpt	
	Mino	110	35°58′7.25"N	137°33′6.50"E	2.65	0.371	Cpt	
	Mino-Ryoke	112	36° 7′25.24"N	137°50′40.80"E	8.06	4.71	Cst	
	Mino-Ryoke	113	36°15′8.23"N	137°50′44.20"E	8.49	2.63	Cpt	
	Mino	114	36°14′52.12"N	137°48′55.67"E	7.40	1.95	Cpt	
	Mino	116	36°11′45.09"N	137°49′29.06"E	7.74	1.37	Cpt	

Area	Geologic unit	Sample No	Latitude	Longitude	CI	GS	Classification	PT
	Mino	120	35°24′51.53"N	137° 8′2.36"E	7.34	1.44	Cpt	
	Mino	124	35°31′47.83"N	137° 7′15.15"E	3.72	0.532	Cpt	238
	Mino	125	35°23′1.19"N	137° 7′19.96"E	3.82	0.535	Cpt	
	Mino	127	35°21′39.62"N	137° 5′36.44"E	4.42	0.427	Cpt	
Area	**Geologic unit**	**Sample No**	**Latitude**	**Longitude**	**CI**	**GS**	**Classification**	**PT**
Ashimidani, Japan	Tanba	130	35° 6′59.79"N	135°37′38.24"E	4.33	0.571	Cpt	
	Tanba	131	35° 6′36.35"N	135°37′56.52"E	4.03	0.408	Cpt	
	Tanba	133	35° 1′45.21"N	135°38′11.17"E	9.37	2.37	Cpt	
	Tanba	135	35° 4′55.85"N	35°37′41.71"E	6.96	1.76	Cpt	
	Tanba	138	35° 5′21.27"N	135°35′43.21"E	7.99	1.67	Cpt	
	Tanba	157	35° 7′17.56"N	135°37′24.98"E	5.76	0.532	Cpt	
	Tanba	159	35° 6′13.62"N	135°37′50.54"E	5.11	0.604	Cpt	
	Tanba	160	35° 6′2.12"N	135°37′50.24"E	5.64	0.744	Cpt	275
	Tanba	162	35° 6′35.08"N	135°37′55.67"E	3.98	0.499	Cpt	273
Ulaanbaatar, Mongolia	Ulaanbaatar	140	47°44′45.12"N	106°42′13.87"E	7.89	1.38	Cpt	
	Ulaanbaatar	142	47°44′22.41"N	106°48′55.90"E	8.59	1.15	Cpt	
	Ulaanbaatar	143	47°26′19.56"N	107°15′11.46"E	8.31	25.3	Cst	
	Ulaanbaatar	145	47°35′15.52"N	107° 7′18.55"E	8.92	1.64	Cpt	
	Ulaanbaatar	146	47°24′40.36"N	106°43′40.88"E	7.86	1.86	Cpt	
	Ulaanbaatar	147	47°23′42.22"N	106°42′3.20"E	9.14	1.15	Cpt	
	Ulaanbaatar	148	47°20′9.61"N	106°40′41.69"E	8.42	2.67	Cst	
	Ulaanbaatar	149	47°17′33.64"N	106°39′35.98"E	7.79	4.33	Cst	
	Ulaanbaatar	152	47°47′14.20"N	107°21′44.60"E	6.08	0.781	Cpt	
	Ulaanbaatar	153	47°47′11.40"N	107°21′16.70"E	5.01	0.492	Cpt	
	Ulaanbaatar	154	47°35′39.60"N	107°18′47.60"E	7.63	3.15	Cpt	
	Ulaanbaatar	155	47°37′54.20"N	106°59′39.60"E	8.87	1.17	Cpt	
	Ulaanbaatar	156	47°34′23.00"N	106°52′26.90"E	2.84	0.447	Cpt	
	Ulaanbaatar	Shrv16	†	†	7.50	2.00	Cst	
	Ulaanbaatar	Shrv21	†	†	8.00	2.50	Cst	
	Ulaanbaatar	Shrv17	†	†	7.50	2.60	Cst	
	Ulaanbaatar	Shrv20	†	†	8.00	2.60	Cst	
	Ulaanbaatar	Shrv18	†	†	8.50	2.80	Cst	
	Ulaanbaatar	Shrv19	†	†	9.00	2.80	Cst	
	Ulaanbaatar	Shrv15	†	†	9.10	3.01	Cst	
	Ulaanbaatar	Shrv13	†	†	7.90	3.02	Cst	
	Ulaanbaatar	Shrv14	†	†	9.80	3.10	Cst	
	Ulaanbaatar	Shrv9	†	†	7.80	3.20	Cst	
	Ulaanbaatar	Shrv10	†	†	9.20	3.20	Cst	
	Ulaanbaatar	Shrv11	†	†	9.30	3.20	Cst	
	Ulaanbaatar	Shrv12	†	†	7.90	3.70	Cst	
	Ulaanbaatar	Shrv8	†	†	8.00	3.80	Cst	
	Ulaanbaatar	Shrv7	†	†	8.30	3.80	Cst	
	Ulaanbaatar	Shrv6	†	†	8.50	5.00	Cst	
	Ulaanbaatar	Shrv1	†	†	9.90	5.05	Cst	
	Ulaanbaatar	Shrv3	†	†	10.00	5.30	Cst	
	Ulaanbaatar	Shrv2	†	†	9.90	5.90	Cst	
	Ulaanbaatar	Shrv4	†	†	10.00	6.05	Cst	
	Ulaanbaatar	Shrv5	†	†	9.50	6.10	Cst	
Anyui, Russia	Samarka	R1*	‡	‡	2.30	0.427	Cpt	
	Samarka	R2*	‡	‡	8.10	1.81	Cpt	
	Samarka	R3	‡	‡	9.10	190	Cst	
	Samarka	R4	‡	‡	9.50	100	Cst	

Area	Geologic unit	Sample No	Latitude	Longitude	CI	GS	Classification	*PT*
	Samarka	R5	‡	‡	9.80	170	Cst	
	Samarka	R6	‡	‡	9.40	70.0	Cst	
	Anyui	R7	‡	‡	9.40	80.0	Cst	
	Anyui	R8	‡	‡	10.10	350	Cst	
	Anyui	R9	‡	‡	8.40	30.0	Cst	
Continued								
	Anyui	R10	‡	‡	9.10	30.0	Cst	
	Samarka	R11*	‡	‡	8.40	1.87	Cpt	
	Samarka	R12*	‡	‡	8.50	1.86	Cpt	
	Samarka	R13*	‡	‡	3.70	0.551	Cpt	
	Samarka	R14*	‡	‡	7.50	0.916	Cpt	

Table 1. Quartz crystallinity index (CI) and grain size (GS) of biogenic chert in the accretionary complexes. Data are shown as three significant digits. Data for Russia, except GS data for the samples with an asterisk, are from Kojima et al. (2008)[14]. Classification: microscopic classification, Crt.: crystalline chert, Cpt.: cryptocrystalline chert, PT: paleotemperature of the mudstone nearby the chert (error: ± 30˚C), †: samples were from the bedded meta-chert of the Gorkhi and Dov formations of the Ulaanbaatar terrane[27] but detail localties are unknown, ‡: see Kojima et al. (2008)[14] for the localities.

The analytical error in the CI measurements of six samples (Sample Nos. 2, 8, 11, 79, 87, and 152) was examined (Fig. 5a). Three powder mounts were prepared for the same sample. The analysis was then repeated five times for each powder mount. As a result, the standard deviation (1σ error) of the CI values for each sample was 0.32–0.52 (average: 0.45) in a total of 15 analyses/sample (Fig. 5a).

GS of the biogenic chert and metachert samples

The measurement of quartz GS was carried out by following the method reported by Mikami et al. (2002)[16]. Apparent GS measured from the thin section or slab surfaces of the biogenic chert or metachert samples is defined as GS herein[16]. The samples were cut in multiple directions and each thin section was observed using an optical microscope. Results revealed that the quartz grains in all samples had not undergone shear deformation. Photomicrographs (taken in cross-polarized light) were used for the GS measurement of crystalline chert (Fig. 3d). For cryptocrystalline chert, the samples were cut into 1-cm square slabs and mirror polished using a diamond paste. The polished surface was etched with 15% hydrofluoric acid for 5 min, and then gold or carbon coating was performed. Subsequently, the gold- or carbon-coated etched surface was observed via SEM (Hitachi High-Tech Corporation, S-3400N and Miniscope TM-1000) installed at the Nagoya University Museum (Fig. 3c).

Further, 10–20 parallel lines were drawn on the obtained SEM image and the distance between each of the point that the lines and grain boundaries intersect was measured. Nearly 300 such measurements were performed for each sample. Histograms and cumulative frequency curves were then plotted, and the GS of the sample was determined as the GS corresponding to a cumulative relative frequency of 0.5[16].

We investigated the analytical errors in GS measurements for each of the six samples (Sample Nos. 2, 8, 11, 79, 87, and 152). A total of six to seven analyses were performed for each sample by three authors. The relative standard deviation of the 1σ error (RSD) of the GS for each sample was 8.46%–11.9% (average: 10.4%) (Fig. 5b).

### PT of mudstone present nearby the biogenic chert and metachert samples

Nine mudstone samples exposed in close proximity to the chert samples were collected, and their PT values were measured using the RSCM geothermometer[24]. Then, the PT values of these mudstone samples were considered to be the same as those of the chert samples, because no fault relationship existed between the chert and mudstone layers. Diamond-polished thin sections were prepared for each mudstone sample and the RSCM were acquired using a spectrometer (Nicolet Almega XR, Thermo Fisher Scientific), installed at the Rock and Mineral Laboratory of Nagoya University. The Raman spectra were obtained in the wavenumber range of 655–1748 cm^{-1}, and ~ 30 carbonaceous grains were detected in each sample. The spectra were decomposed into three to five peaks using PeakFit 4.12 (SeaSolve Software Inc.). Peak fitting was performed for each spectrum and mean values and standard deviations of FWHM-D1 were determined for each sample. The value "FWHM-D1" is the full width at half maximum of the peak named D1 occurring at ~ 1350 cm^{-1} in the spectra. Data deviating more than 2σ from the mean were omitted, and final means were determined using only remaining data. Then, temperatures were calculated using the following eqation [24]. The analytical error in the temperature measurement was ± 30 °C[24].

$$T\left(^{\circ}C\right) = -2.15(\text{FWHM} - \text{D1}) + 478$$

Results
Relationship between CI and GS

The data used in this study are provided in Table 1, and Fig. 6a shows a plot of the relationship between CI and GS. Data obtained from Japan, Russia, and Mongolia showed similar trends (Fig. 6a). Specifically, CI and GS
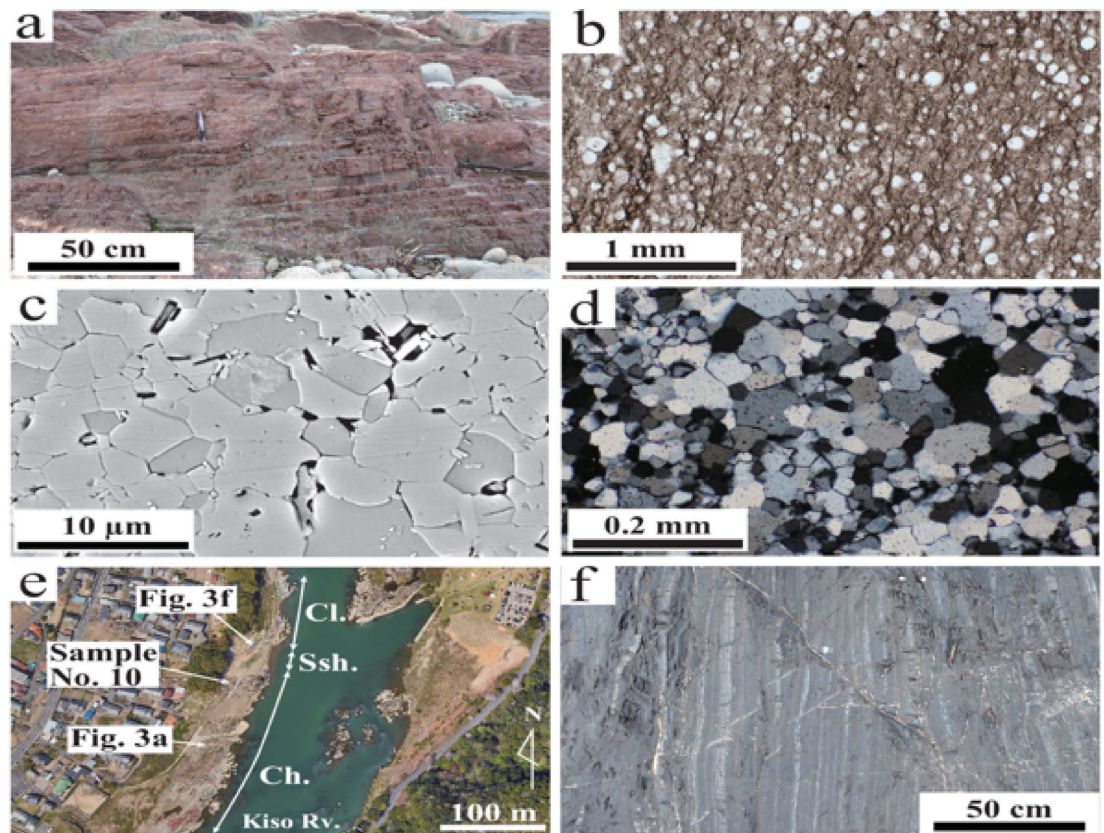
Fug. 3

Fig. 3. (**a**) Field occurrence of the Upper Triassic bedded biogenic chert in the Mino belt in Chubu province, Japan (sample No. 10). Refer to Fig. 3e and Table 1 for locality details. (**b**) Optical photomicrograph (obtained in plane polarized light) of the Upper Triassic biogenic chert including numerous radiolarian tests (white spots in the picture). Plane polarized light. (**c**) Backscattered scanning electron image of a bedded metachert sample obtained from the Ryoke belt in Chubu province, Japan. (**d**) Optical photomicrograph (obtained in cross-polarized light) of a bedded metachert sample composed of crystalline quartz obtained from the Ryoke belt in Chubu province, Japan. (**e**) Satellite image of the locality around sample No. 10. The image was taken from Google Earth Pro (https://www.google.com/permissions/geoguidelines/?hl=ja). Following the oceanic plate stratigraphy, the chert layers are overlain by siliceous shale and clastic rocks. Ch.: bedded radiolarian chert, Ssh.: siliceous shale, Cl.: clastic rocks, Loc.: locality, Rv: river. (**f**) Field observation of the alternating layers of sandstone and mudstone beds overlying the radiolarian chert beds. The locality is shown in Fig. 3e.

showed in a logarithmic relationship when GS was low (roughly cryptocrystalline). Further, CI was stabilized at almost 8.0–10 and GS increased (roughly crystalline).

Next, we discuss the range where a logarithmic relationship was observed between CI and GS holds. This study examined the group of datapoints showing the highest logarithmic correlation coefficient (R value) between CI and GS by adding datapoints in the ascending order of GS, starting with the smallest GS (0.306 μm for the sample No. 44) (Fig. 6b; Table 2). The R value increased with increasing number of datapoints, reaching the maximum for the group of datapoints with GS ≤ 1.94 μm. Thereafter, the R value gradually decreased as the number of datapoints increased. For the group with GS ≤ 1.94 μm, the approximation relation between CI and GS was as follows (Fig. 6):

$$CI = 3.57 \ln (GS) + 6.46 \, (R = 0.915). \tag{1}$$

The correlation coefficient of this equation is not low; therefore, this group can be regarded as the one that shows a logarithmic relationship between CI and GS (Fig. 6b).

Relationship between GS or CI and PT

This section discusses the relationship between CI or GS and PT for the group of datapoints for which Eq. 1 holds (the group with GS ≤ 1.94 μm) for the samples obtained from Japan. The investigated mudstone and chert samples have a conformable relationship and the PT experienced by both the rock types over geologic time was assumed to be nearly identical (Fig. 3a, e, and f). Therefore, the PT of the mudstone outcrops present near the chert outcrops, as measured using the RSCM geothermometer, was considered to be the PT of the chert samples.
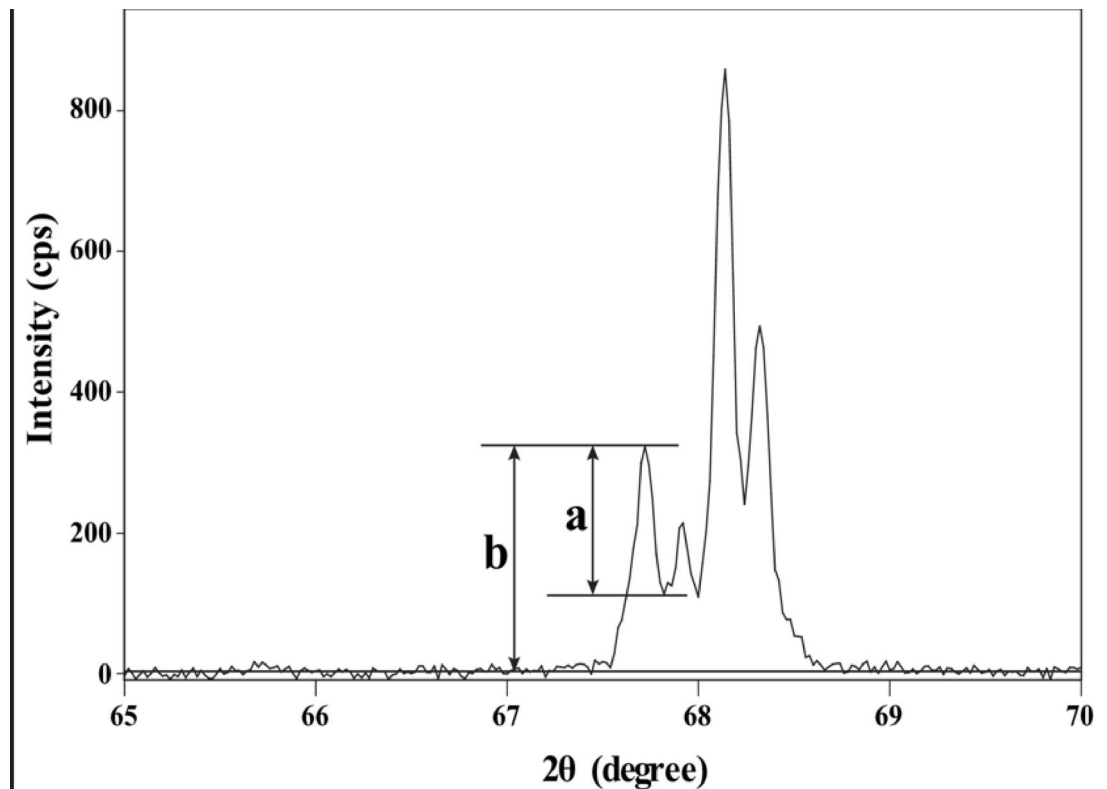
Fig. 4. Quartz (212) peak at $2\theta = 67.74°$ of the standard sample obtained from the Minas Gerais, Brazil. The values "a" and "b" determined by Murata and Norman (1976)[3] are shown.

Furthermore, CI and GS were found to increase regularly with increasing PT, with a positive linear relationship observed between CI and PT (Fig. 7a) and a logarithmic relationship observed between GS and PT (Major Points) (Fig. 7b). Based on the actual measurements of CI for the chert samples and PT for the adjacent mudstone samples, the following equation between CI and PT was established (Fig. 7a):

$$CI = 0.0546 T_{CI} - 9.28 \, (R = 0.942), \tag{2}$$

where T_{CI} is a PT value (in °C) corresponding to a CI value.
From Eq. 2, PT (T_{CI}) was expressed as follows:

$$T_{CI} = 18.3 \, CI + 170. \tag{3}$$

For the relationship between GS and PT, based on actual observations, the following equation was derived (Fig. 7b):

$$GS = 0.0182 \exp\left(0.0141 T_{GS}\right) (R = 0.929), \tag{4}$$

where T_{GS} is a PT value (in °C) corresponding to a GS value.
Then, Eq. 4 was modified as follows:

$$T_{GS} = 71.0 \ln GS + 285. \tag{5}$$

Discussion
Spatiotemporal commonality of the CI versus GS relationship
In the circum-Pacific orogenic belt, the chert samples obtained from the Chubu province and Ashimidani area were assigned to the Triassic–Jurassic and Permian, respectively[25–29]. The chert samples obtained from the Anyui area, located ~ 1500 km north of the study areas in Japan, dated back to the Triassic–Jurassic period[20]. In the Central Asian orogenic belt of the Mongolia, the chert samples obtained from the Ulaanbaatar area contained microfossils from the Silurian and Devonian periods[22]. Samples obtained from the investigated regions of Japan, Russia, and Mongolia showed varying ages and places of origin (Fig. 2).

Some geological units analyzed in this study underwent various degrees of metamorphism and alteration and were intruded by dikes and mineral veins. Furthermore, chert exposed near basaltic rocks might have been of submarine hydrothermal origin. This study focused on the relationship between the CI, GS, and PT of biogenic chert through the diagenesis and metamorphism process, and factors that may affect the CI and GS data other than
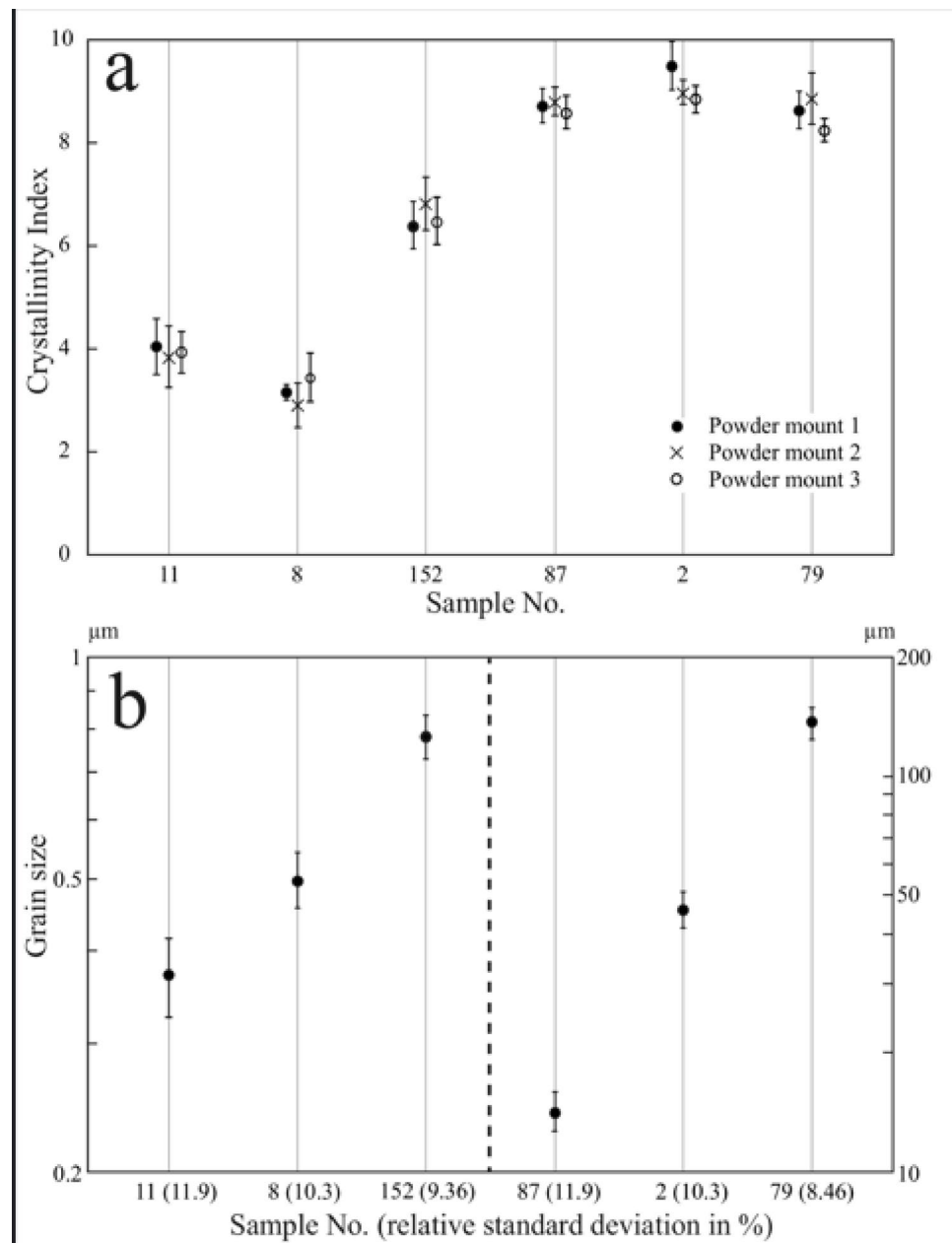
Fig. 5. (**a**) Results of the repeated CI measurements of quartz in the biogenic chert and metachert samples. The standard deviations of the five analyses for each powder mount are shown with error bars. (**b**) Results of repeated GS measurements of quartz in the biogenic chert and metachert samples. The standard deviations of six and seven analyses by three authors for each sample are shown with error bars. The left Y-axis is for sample Nos. 11, 8, and 152, and the right Y-axis is for sample Nos. 8, 7, and 79. Relative standard deviations for each sample are also shown with three significant digits. No.: number.

temperature were excluded as much as possible. For example, samples that may have undergone hydrothermal alteration (e.g., those located near the thin muddy films intercalated with chert layers, those near large veins, and those containing many quartz microveins) were excluded in this study. Samples, exposed near the basaltic rocks, without any fossil remains were avoided, considering the possibility of them being hydrothermal chert. It is widely known that the dynamic recrystallization of quartz can lead to GS reduction[34]. Consequently, all examined chert samples were confirmed to be undeformed. All data obtained from Japan, Russia, and Mongolia showed the same trend each other, i.e., CI and GS showed in a logarithmic relationship when GS was low, and CI were stabilized at almost 8.0–10 when GS was high. Therefore, the relationship between CI and GS discussed herein is probably a general principle for biogenic chert, regardless of rock age and place of origin (Figs. 2 and 6a).
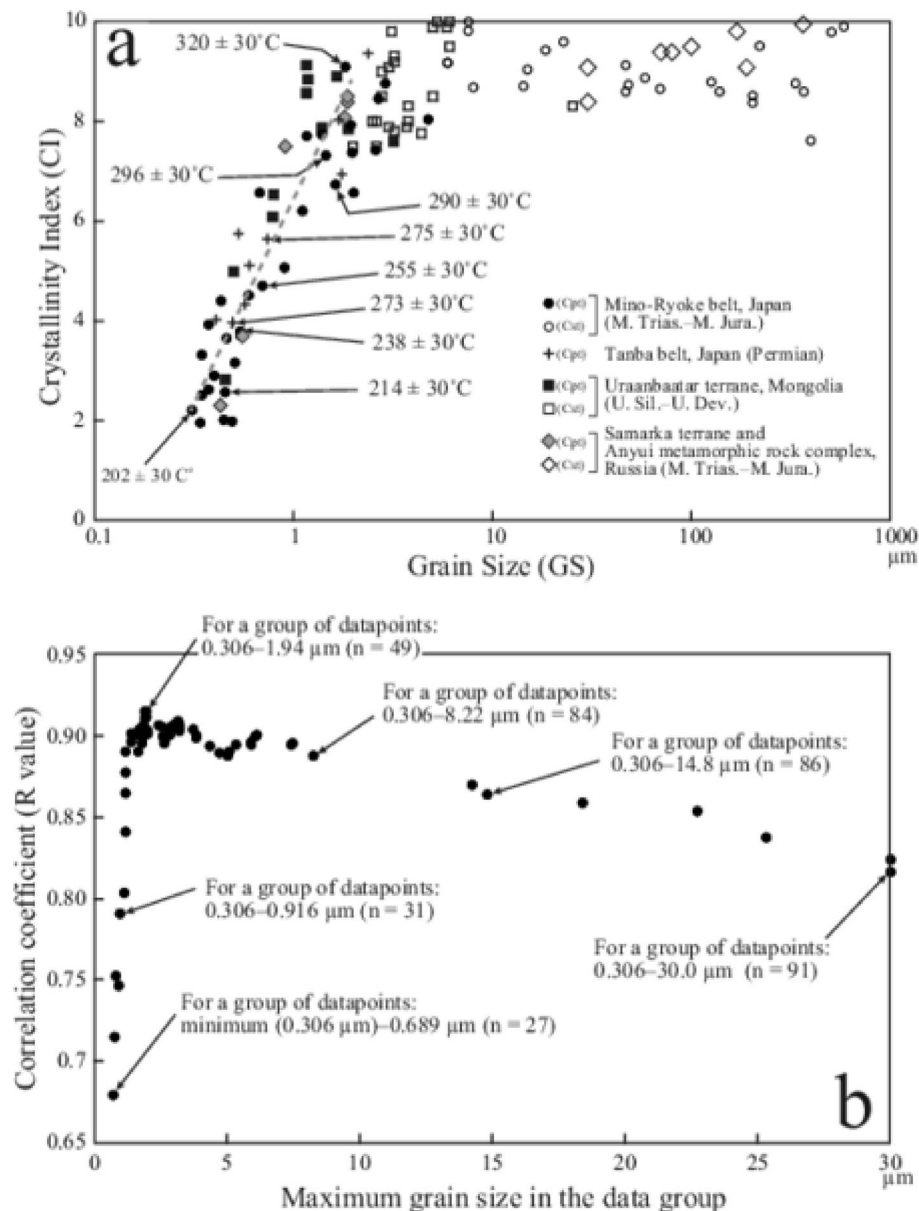
Fig. 6. (**a**) Relationship between the quartz crystallinity index (CI) and grain size (GS) of the biogenic chert and metachert samples. The dotted line is the approximate line of CI vs. GS (for the group of datapoints with GS ≤ 1.94 μm). Paleotemperatures of the mudstone samples present nearby the chert samples are also shown. Cpt: cryptocrystalline chert, Cst: crystalline chert, M: Middle, U: Upper, Sil.: Silurian, Dev.: Devonian, Trias.: Triassic, Jura.: Jurassic. (**b**) Relationship between the correlation coefficient (R value) of CI and GS and the maximum crystal size (μm) in the group of datapoints. Refer to Table 2 for the data. GS: grain size, n: number of the data.

Spatial consistency verification of the derived equations

The derived equations were obtained empirically from independent observations of the CI–GS, CI–PT, and GS–PT relationships. The relationship between CI or GS and PT was derived from data obtained from Japan, and can be applied to the Jurassic accretionary complex in Japan. However, it still remains questionable whether the relationship between CI or GS and PT is also generally applicable. If these relationships are applicable to the other regions, it should be in concordant with the relationship between CI and GS which is a general principle of the biogenic chert regardless of age and place. Here, to assess the spatial consistency of these relationships, Eqs. 1, 3, and 5 were used to examine whether the correlation between CI and GS and that between CI or GS and PT aligned with each other. The relationship between T_{GS} corresponding to any GS value ($T_{GS}^{\dagger}$) and T_{CI} corresponding to a CI value calculated by substituting any GS value into Eq. 1 ($T_{CI}^{\dagger}$) is shown in Table 3. If Eq. 1—derived from data obtained from Japan, Russia, and Mongolia—and Eqs. 3 and 5—derived from

Sample No. of maximum GS (A) in the group	CI of (A)	GS of (A)	R value	Data No
106	4.72	0.689	0.6799	27
160	5.64	0.744	0.7160	28
152	6.08	0.781	0.7529	29
7	5.10	0.900	0.7471	30
R14*	7.50	0.916	0.7915	31
96	6.23	1.10	0.8038	32
147	9.14	1.15	0.8407	33
142	8.59	1.15	0.8647	34
97	7.73	1.15	0.8782	35
155	8.87	1.17	0.8915	36
116	7.74	1.37	0.8967	37
140	7.89	1.38	0.9025	38
120	7.34	1.44	0.9020	39
93	6.77	1.62	0.8910	40
145	8.92	1.64	0.9009	41
138	7.99	1.67	0.9040	42
135	6.96	1.76	0.8965	43
R2*	8.10	1.81	0.9000	44
25	9.12	1.82	0.9070	45
R12*	8.50	1.86	0.9110	46
146	7.86	1.86	0.9115	47
R11*	8.40	1.87	0.9145	48
16	7.94	1.94	0.9150	49
114	7.40	1.95	0.9122	50
105	6.60	1.99	0.9031	51
Shrv16	7.50	2.00	0.9019	52
133	9.37	2.37	0.9070	53
Shrv21	8.00	2.50	0.9056	54
20	7.45	2.55	0.9004	55
Shrv17	7.50	2.60	0.8961	56
Shrv20	8.00	2.60	0.8957	57
113	8.49	2.63	0.8976	58
Sample No. of maximum GS (A) in the group	**CI of (A)**	**GS of (A)**	**R value**	**Data No**
148	8.42	2.67	0.8991	59
Shrv18	8.50	2.80	0.9006	60
Shrv19	9.00	2.80	0.9035	61
95	8.79	2.86	0.9056	62
Shrv15	9.10	3.01	0.9082	63
Shrv13	7.90	3.02	0.9060	64
Shrv14	9.80	3.10	0.9094	65
154	7.63	3.15	0.9054	66
Shrv9	7.80	3.20	0.9026	67
Shrv10	9.20	3.20	0.9050	68
Shrv11	9.30	3.20	0.9074	69
Shrv12	7.90	3.70	0.9037	70
Shrv7	8.30	3.80	0.9006	71
Shrv8	8.00	3.80	0.8993	72
149	7.79	4.33	0.8940	73
112	8.06	4.71	0.8898	74
Shrv6	8.50	5.00	0.8879	75
Shrv1	9.90	5.05	0.8912	76
Shrv3	10.00	5.30	0.8945	77
23	9.20	5.88	0.8947	78
Shrv2	9.90	5.90	0.8972	79
Shrv4	10.00	6.05	0.8998	80
Shrv5	9.50	6.10	0.9008	81
Continued				

Sample No. of maximum GS (A) in the group	CI of (A)	GS of (A)	R value	Data No
94	8.30	7.37	0.8945	82
4	9.84	7.46	0.8960	83
31	8.13	8.22	0.8883	84
87	7.85	14.2	0.8702	85
6	9.05	14.8	0.8638	86
5	9.44	18.4	0.8588	87
38	9.61	22.7	0.8540	88
143	8.31	25.3	0.8384	89
R9	8.40	30.0	0.8235	90
R10	9.10	30.0	0.8169	91

Table 2. The data for the Fig. 6b. Thick border: plotted data for Fig. 3b. R value: correlation coefficient, Data No.: number of the data for log approximation.

data obtained from only Japan—are inconsistent, $T_{CI}^{\dagger} \neq T_{GS}^{\dagger}$ is expected. Further, if the Eqs. 1, 3, and 5 match, $T_{CI}^{\dagger} = T_{GS}^{\dagger}$ should apply.

Therefore, $T_{CI}^{\dagger} = 0.920 \, T_{GS}^{\dagger} + 26.0$ was obtained as the correlation equation for $T_{CI}^{\dagger}$ and $T_{GS}^{\dagger}$, with a slight deviation from the ideal equation ($T_{CI}^{\dagger} = T_{GS}^{\dagger}$) (Fig. 8a). This deviation might be attributed to CI and GS measurement errors, as discussed later. To assess the similarity between these two equations, cosine similarity can be used, which evaluates the parallelism of two vectors. Cosine similarity is defined as the cosine value of the angle between two vectors; for example, a cosine similarity of 1 indicates that the vectors are parallel (the angle between the two vectors is 0°), and a cosine similarity of 0 indicates that they are orthogonal (the angle between the two vectors is 90°). As the extent of parallelism between the two vectors increases the cosine similarity value approaches 1. The cosine similarity between the equations $T_{CI}^{\dagger} = 0.920 \, T_{GS}^{\dagger} + 26.0$ and the ideal equation ($T_{CI}^{\dagger} = T_{GS}^{\dagger}$) was almost 1 (0.999). Therefore, it was concluded that the slopes of the two equations for $T_{CI}^{\dagger}$ and $T_{GS}^{\dagger}$ were nearly identical. Moreover, the difference between $T_{CI}^{\dagger}$ and $T_{GS}^{\dagger}$ within the range investigated in this study (GS: 0.4–1.9 μm) was small: 8.4°C for $T_{GS}^{\dagger} = 220$°C and 0.42°C for $T_{GS}^{\dagger} = 331$°C (Fig. 8a). Thus, the relationship between CI, GS, and PT proposed in this study apparently hold well within the range of 220°C–330°C.

Figure 8b shows the T_{CI} vs. T_{GS} plots of the biogenic chert and metachert samples obtained from actual CI and GS values for Japan, Russia, and Mongolia using Eqs. 3 and 5. The data scattered along the ideal line ($T_{CI} = T_{GS}$), with the standard deviation of the difference between T_{CI} and T_{GS} being 17.9°C (1 σ) and 35.9°C (2 σ). Although this seems to be the error limit in the current investigation, the study clearly outlines the relationship between quartz CI, GS, and PT in the cryptocrystalline region. Furthermore, using the method presented in this study, the reliability of the results can be assessed by comparing T_{CI} and T_{GS}.

Limitations of this study and future aspects

The previous section confirms the spatial consistency of the CI–GS, CI–PT, and GS–PT relationships; however, the present data still show regional bias. This study was based on the data obtained from four regions in East Asia. Further collection of data for biogenic chert in other regions will refine the correlations among CI, GS, and PT. Notably, the mutual relationship between CI, GS, and PT proposed herein is only applicable for the group of datapoints with GS ≤ 1.94 μm. CI early reaches its maximum at GS = 1.94 μm, and for the group of datapoints with GS > 1.94 μm, CI and GS show a linear relationship (Fig. 6b). Therefore, the equations proposed in this study are applicable only to unmetamorphosed and weakly metamorphosed chert and cannot be applied to chert in the "metamorphic belt." To estimate PT from quartz GS (in the range of 2.9–67 μm), the equation T (°C) = 39.7 ln (quartz GS) + 204 has been proposed in a study on low-grade metamorphic rocks in the Sambagawa belt, southwest Japan[6]. This equation, in combination with the equations derived in the present study, can form a powerful tool for clarifying the tectonothermal histories of metamorphic belts. However, this may not be always an easy and inexpensive method because it involves electron backscatter diffraction analysis etc. To clarify the tectonothermal histories of broader regions on Earth, the development of a simple method for estimating PT from the GS of crystalline chert using an optical microscope, as demonstrated in this study, might be important as well.

In the method proposed herein, the smaller GS values lead to larger differences between $T_{CI}^{\dagger}$ and $T_{GS}^{\dagger}$ (Fig. 8a). This might be attributed to CI and GS measurement errors. The standard deviation of the CI values in this study was 0.32–0.52 (1σ error), which might not be strictly small (Fig. 5a). Moreover, the microscopic examination of GS is a subject to observer bias; consequently, the RSD of GS in this study was 8.46%–11.9% and the average was 10.4% (Fig. 5b). In the low-temperature range, especially, these measurement errors of CI and GS may have a remarkable impact on PT estimation. In the future, by developing a method for accurately measuring a GS of < 1 μm or through some correction formula, the determination of more accurate values of T_{CI} and T_{GS} will be possible in the low-temperature range.

The results of this study were empirically derived and are not supported by theoretical background. It has been reported that when the spatial distribution of garnet in metamorphic rocks is uniform and sufficient time has elapsed for equilibrium to be reached, the GS distribution of garnet is consistent with the Lifshitz–Slyozov–Wagner distribution of Ostwald ripening[35]. Further, it has been revealed that higher temperatures lead to higher
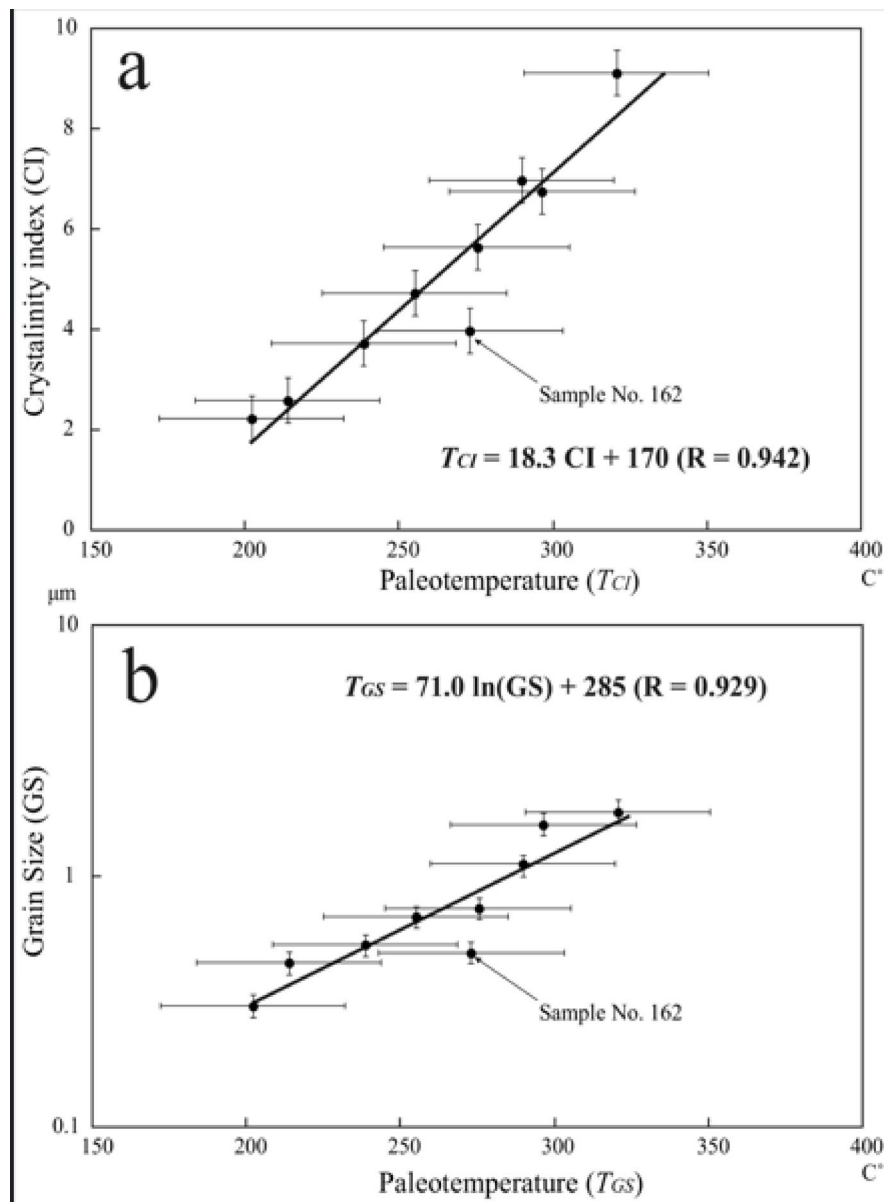
Fig. 7. (**a**) Relationship between the quartz crystallinity index (CI) of chert vs. paleotemperature of mudstone present nearby the chert outcrops. Error bars for quartz crystallinity and paleotemperature denote ± 0.45 and ± 30 °C respectively. (**b**) Relationship between the quartz grain size (GS) of chert vs. paleotemperature of mudstone present nearby the chert outcrops. Error bars for GS and paleotemperature denote ± 10% of the data and ± 30 °C respectively. CI: quartz crystallinity index, GS: quartz grain size.

conversion rates of amorphous silica into quartz[7–11]. In future investigations, consideration of concepts such as Ostwald ripening, silica phase transformations, crystal growth under stress, can provide important insights into the theoretical understanding of the relationship between quartz CI, GS, and PT.

The XRD intensity of quartz powder is known to be the highest when the particle size is 1–10 μm; the intensity decreases when the particle size is < 1 μm or > 10 μm[36]. Herein, we determined the chert CI using powder samples with a mean particle size of 1–20 μm; however, we acknowledge that some larger/smaller particles contaminated the samples. For increased sufficient X-ray intensity, paying close attention to the particle size of the sample powder is necessary.

Herein, PT of the mudstone sample obtained from the mudstone outcrop overlying the chert outcrop was that of the chert sample and the correlation between CI and GS vs. PT was investigated. Therefore, highly positive correlations (R > 0.93) were observed between CI and PT and between GS and PT (Fig. 7). However, a sample (No. 162) appears to lie outside the approximate lines of CI or GS vs. PT, toward the high-temperature side (Fig. 7). The mudstone sample for which PT was estimated was located only 100 m away from the chert outcrop of the sample No. 162. No fault rocks were recognized between them, and these chert and mudstone

Any GS (µm)	CI*	$T_{GS}{}^{\dagger}$ (C°)	$T_{CI}{}^{\dagger}$ (C°)	Difference between $T_{GS}{}^{\dagger}$ and $T_{CI}{}^{\dagger}$
0.4	3.19	219.94	228.36	8.41
0.5	3.99	235.79	242.93	7.15
0.6	4.64	248.73	254.85	6.11
0.7	5.19	259.68	264.92	5.24
0.8	5.66	269.16	273.64	4.48
0.9	6.08	277.52	281.33	3.82
1.0	6.46	285.00	288.22	3.22
1.1	6.80	291.77	294.44	2.68
1.2	7.11	297.94	300.13	2.18
1.3	7.40	303.63	305.36	1.73
1.4	7.66	308.89	310.20	1.31
1.5	7.91	313.79	314.71	0.92
1.6	8.14	318.37	318.92	0.55
1.7	8.35	322.67	322.88	0.21
1.8	8.56	326.73	326.62	0.11
1.9	8.75	330.57	330.15	0.42

Table 3. Consistency of $T_{GS}{}^{\dagger}$ and $T_{CI}{}^{\dagger}$. CI*: CI calculated by assigning any GS into Eq. 1. $T_{GS}{}^{\dagger}$: T_{GS} calculated by assigning any GS into Eq. 5. $T_{CI}{}^{\dagger}$: T_{CI} calculated by assigning CI* into Eq. 3.

outcrops seemed to be in a conformable relationship. Further, the estimated reason for high PT of sample No. 162 was investigated.

A major thrust fault dividing the geological units existed just 200 m to the north of the chert and mudstone outcrops[29]. In general, the temperature around a fault rises owing to frictional heat and hot fluids entering the cracks created by fault activity, thereby causing hydrothermal alteration of the surrounding rocks. A previous study revealed that the fault gouge around the Nankai Trough was heated to > 300 °C using a vitrinite reflectance geothermometer[37]. Therefore, the mudstone sample might have been affected a local thermal event owing to the thrust fault activity. This might be the reason for the deviation from the approximate line. The deviation of the sample No. 162 from the approximate line is likely owing to higher sensitivity of carbonaceous material crystallinity to PT than quartz CI or GS. As the regression equations of CI or GS vs. PT were mostly the same even when including or excluding the mudstone sample data, this study presented them as well (Fig. 7). However, in future, when applying the method proposed in this study, paying attention to the surrounding geological structure, especially the fault distribution around the sampling locations to avoid the thermal influence of fault activities on analysis outcomes, is necessary.

According to a study of chert obtained from the Jurassic accretionary complex in Japan (Ashimidani area), a logarithmic relationship between CI and GS has been suggested for GS < 10 µm using the conodont color index, further suggesting an increase in CI and GS with increasing PT[16]. The results of this study are supported by these observations. Mikami's results lacked the precision necessary for reliable PT estimation; however, this study provides high-precision empirical equations that offer a robust tool for estimating the PT of biogenic chert in the cryptocrystalline region.

In geosciences, mineral geothermometers, such as garnet–biotite thermometers, chlorite thermometers, and illite/carbonaceous material crystallinity thermometers, have been widely applied as powerful tools for understanding Earth's history[24,38–41]. Minerals in pelitic rocks are commonly used as geothermometers for sedimentary rocks (including metamorphic rocks). For example, the PT estimation of rocks in accretionary complexes has helped clarify subduction and accretionary systems[42]. However, in regions where erosion is inactive and alluvial sediments mostly cover the rocks, no pelitic rocks are exposed; only relatively hard erosion-resistant biogenic chert and metachert rocks are present (Fig. 1). The method proposed herein has significant implications for geothermometers in regions with limited pelitic-rock exposure. In future, the methodology developed in this study can become an essential tool for geologists working in regions where pelitic rocks are inaccessible, improving our understanding of tectonic processes in underexplored geological settings. For example, Northeast Eurasia is considered to have formed by the collision of the Siberian and South Mongolian continents. Further, the boundary between the two continents is defined as the Mid-Mongolian Tectonic Line (MMTL)[23,43]. The southern part of Siberia (Carboniferous accretionary complex; Khangai–Daur belt) appears to show an increase in the metamorphic grade toward the MMTL, and its metamorphism is indispensable for understanding the tectonics of Northeast Eurasia[44]. However, the Khangai–Daur belt hardly exposes pelitic rocks, leaving its metamorphism poorly understood. The application of the method proposed herein as well as future geothermometers developed based on crystalline quartz to biogenic chert in the Khangai–Daur belt will probably promote greatly the study of the tectonics of Northeast Eurasia. Furthermore, a noteworthy aspect of this study is that it enables the reliable and easy estimation of PT using inexpensive equipment such as optical microscopes, SEM devices, and XRD devices. The proposed method is expected to significantly contribute to study of geology around the world for elucidating Earth's history.

While the study provides a reliable method for estimating PT in the range of 220 °C–330 °C, its applicability at higher temperatures or other geological environments requires further investigation. Future research should

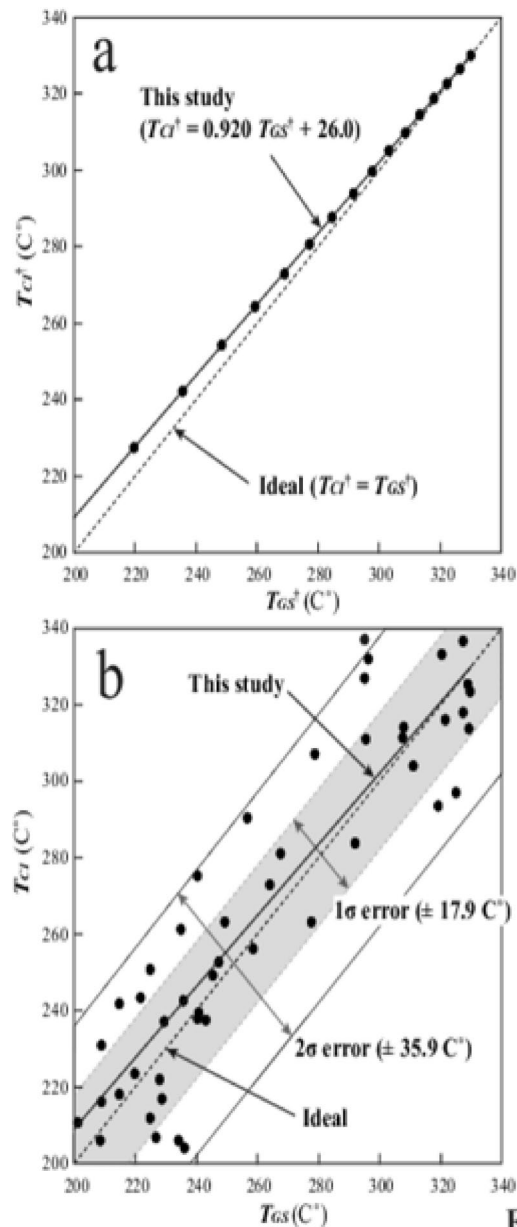**Fig. 8**. (**a**) Comparison between the result of this study ($T_{CI}{}^{\dagger} = 0.920\ T_{GS}{}^{\dagger} + 26.0$) and the ideal correlation equation ($T_{CI} = T_{GS}$). (**b**) Actual plots of T_{CI} vs. T_{GS} obtained in this study.

focus on expanding the temperature range for quartz geothermometers, incorporating samples from different geological settings, and refining the CI–GS correlation in cryptocrystalline chert for broader applications.

Glossary of technical terms

Pelitic rocks: Sedimentary rocks composed of clay- or mud-size particles and their metamorphosed forms.

Alluvial sediments: The latest sediments carried by streams and deposited where the stream slows down.

Chert: Fine-grained sedimentary rock composed of microcrystalline or cryptocrystalline quartz.

Metachert: Metamorphosed chert.

Radiolarians: A single-celled marine planktonic eukaryotic organism with a diameter of <1 mm and a skeleton composed of silica.

Diagenesis: A process by which sediments solidify to form sedimentary rocks.

Accretionary complex: A geological unit formed when sediments and other materials on an oceanic plate are accreted to the continental side after oceanic plate subduction.

Cryptocrystalline: A rock texture composed of very small crystals. Even under an optical microscope, the crystal shape is hardly recognized.

Crystalline: A rock texture composed of crystals that can be recognized under an optical microscope.

Microfossils: Fossils, which have a size of typically less than a few millimeters, that require a microscope to be observed.

Conodonts: "Tooth-like" microfossils of marine jawless vertebrates.

Data availability

All data generated or analyzed during this study are included in this published article.

References

1. Grotzinger, J., Jordan, H. T., Press, F. & Siever, R. *Understanding earth, 5th edition*. 579p (W. H. Freeman and Company, 2007).
2. Boggs, S. Jr. *Principles of Sedimentology and Stratigraphy, 4th edition*. 662p (Pearson Prentice Hall, 2006).
3. Murata, K. J. & Norman, M. B. An index of crystallinity for quartz. *Am. J. Sci.* **276**, 1120–1130 (1976).
4. Hattori, I. *Chert and siliceous sediments: their depositional processes and diagenesis*. 272p (Kinmiraisha, 2008).
5. Hein, J. R., Vallier, T. L. & Allan, M. A. Chert petrology and geochemistry, Mid-pacific Mountains and Hess rise, deep sea drilling project leg 62. *Init. Rep. DSDP* **42**, 711–748 (1981).
6. Hara, H., Mori, H., Tominaga, K. & Nobe, Y. Progressive low-grade metamorphism reconstructed from the Raman spectroscopy of carbonaceous material and an EBSD analysis of quartz in the Sanbagawa metamorphic event, central Japan. *Minerals* **11**, 854. https://doi.org/10.3390/min11080854 (2021).
7. Mizutani, S. Progressive ordering of cristobalitic silica in the early stage of diagenesis. *Contrib. Mineral. Petrol.* **61**, 129–140 (1977).
8. Ernst, W. G. & Calvert, S. E. An experimental study of the recrystallization of porcellanite and its bearing on the origin of some bedded cherts. *Am. J. Sci.* **267A**, 114–133 (1969).
9. Kano, K. & Taguchi, K. Experimental study on the ordering of opal-CT. *Geochem. J.* **16**, 33–44 (1982).
10. Mitsui, K. & Taguchi, K. Silica mineral diagenesis in Neogene Tertiary shales in the Tempoku district, Hokkaido Japan. *J. Sediment. Petrol.* **47**, 158–167 (1977).
11. Reich, V. & von Rad, U. Silica diagenesis in the Atlantic Ocean: diagenetic potential and transformations. In *Deep Sea Drilling Results in the Atlantic Ocean: Continental Margins and Paleoenvironment* 315–340 (Am. Geophys. Union, 1979).
12. Mizutani, S. Kinetic aspects of diagenesis of silica in sediments. *J. Earth Sci. Nagoya Univ.* **15**, 99–111 (1967).
13. Mizutani, S. Silica minerals in the early stage of diagenesis. *Sedimentology* **15**, 419–436 (1970).
14. Murata, K. J. & Nakata, J. K. Cristobalitic stage in the diagenesis of diatomaceous Shale. *Science* **184**, 567–568 (1974).
15. Inoue, M. Crystallization and recrystallization of siliceous sponge spicules in some marine sediments of Japan. *J. Geol. Soc. Jap.* **79**, 277–286 (1973).
16. Mikami, T., Mukai, K., Tokuta, N. & Imoto, N. Relationships among quartz crystallinity index, grain size of quartz, and conodont color alteration index of bedded cherts in the Tanba Belt Southwest Japan. *J. Geol. Soc. Japan* **108**, 806–812 (2002).
17. Sharav, D., Tsukada, K., Oyunchimeg, T., Manchuk, N. & Otgonbaatar, D. Quartz crystallinity of radiolarian chert in the Ulaanbaatar terrane. *Bull. Geol. Mongolia* **61**, 186–193 (2019).
18. Geological Survey of Japan (ed.) *Seamless Digital Geological Map of Japan 1: 200, 000*. (Geol. Surv. Jap., 2020).
19. Khanchuk, A. I., Ratkin, V. V., Ryazantseva, M. D., Golozubov, V. V. & Gonokhova, N. G. *Geology and Mineral Deposits of Primorsky Krai (Territory)*. (Far East Geol. Inst., Rus. Academy Sci., 1996).
20. Kojima, S. et al. Geological relationship between Anyui Metamorphic Complex and Samarka terrane Far East Russia. *Island Arc* **17**, 502–516 (2008).
21. B. Dorjsuren, B. Bujinlkham, Ch. Minjin & Tsukada, K. Geological setting of the Ulaanbaatar terrane in the Hangay-Hentey zone of the Devonian accretionary complex, central Asian Orogenic belt. Tomurhuu, D., Natal'in, B.A., Ariunchimeg, Y., Khishigsuren, S., and Erdenesaikhan, G. (eds.), *Structural and Tectonic Correlation Across the Central Asia Orogenic Collage: Implications for Continental Growth and Intracontinental Deformation (Second International Workshop and Field Excursions for IGC Project 480), Abstract and Excursion Guidebook*, 39–42 (Institute of Geol. Min. Res., Mongolian Academy of Sci., 2006).
22. Kurihara, T. et al. Upper Silurian and Devonian pelagic deep-water radiolarian chert from the Khangai-Khentei belt of Central Mongolia: evidence for Middle Paleozoic subduction–accretion activity in the Central Asian Orogenic Belt. *J. Asian Earth Sci.* **34**, 209–225 (2009).
23. Umeda, K. et al. Permian-Triassic adakitic igneous activity at Northern Mongolia: Implication for Permian-Triassic subduction system at the Siberian continental margin. *J. Geodynam.* https://doi.org/10.1016/j.jog.2022.101918 (2022).
24. Kouketsu, Y. et al. A new approach to develop the Raman carbonaceous material geothermometer for low-grade metamorphism using peak width. *The Island Arc* **23**, 33–50 (2014).
25. Kano, K. Stratigraphy of the upper Paleozoic-Mesozoic strata in the northern Kiso-Azusagawa district Nagano prefecture. *J. Geol. Soc. Jap.* **81**, 285–300 (1975).
26. Otsuka, T. Upper Paleozoic and Mesozoic strata in the northeastern part of the Mino Terrane, Nagano prefecture, central Japan. *J. Geol. Soc. Jap.* **91**, 583–598 (1985).
27. Otsuka, T. Deformation of the Mesozoic strata in the northeastern part of the Mino-Ryoke Terrane, Nagano prefecture, central Japan. *News Osaka Micropleontol Sp.* **7**, 187–196 (1986).
28. Takeuchi, M., Nakano, S., Harayama, S. & Otsuka, T. *Geology of the Kiso-Fukushima district with Geological Sheet Map at 1:50,000*. 94p (Geol. Surv. Jap., 1998).
29. Imoto, N., Shimizu, D., Musashino, M. & Ishida, S. *Geology of the Kyoto seihokubu district with Geological Sheet Map at 1:50,000*. 84p (Geol. Surv. Jap., Tsukuba, 1989).
30. Matsuda, T. & Isozaki, Y. Well-documented travel history of Mesozoic pelagic chert in Japan: From remote ocean to subduction zone. *Tectonics* **10**, 475–499 (1991).
31. Kojima, S. et al. Pre-Cretaceous accretionary complexes. in *The Geology of Japan*, 61–100 (Geol. Soc. London, London, 2016).
32. Isozaki, Y. Jurassic accretion tectonics of Japan. *Island Arc* **6**, 25–51 (1997).
33. Maruyama, S. et al. A new perspective on metamorphism and metamorphic belts. *Gondwana Res.* **18**, 106–137 (2010).
34. Passchier, C.W. *Microtectonics*. 289p (Springer, 1995).
35. Miyazaki, K. Textural evolution of metemorphic rocks due to Ostwald ripening. *J. Min. Soc. Jap.* **24**, 107–115 (1996).
36. Shimazu, M. Relationship between the particle size and the X-ray diffraction intensity of the quartz powders treated with NaOH solution, and the structural disturbance of crushed microparticles of quartz. *J. Min. Soc, Jap.* **6**, 259–276 (1963).
37. Sakaguchi, A. et al. Seismic slip propagation to the updip end of plate boundary subduction interface faults: vitrinite reflectance geothermometry on integrated ocean drilling program NanTro SEIZE cores. *Geology* **39**, 395–398 (2011).
38. Ferry, J. M. & Spear, F. S. Experimental calibration of the partitioning of Fe and Mg between biotite and garnet. *Cont. Mineral. Petrol.* **66**, 113–117 (1978).
39. Kisch, H. J. Illite crystallinity and coal rank associated with lowest-grade metamorphism of the Taveyanne greywacke in the Helvetic zone of the Swiss Alps. *Eclogae geol. Helv.* **73**, 753–777 (1980).

40. Hara, H. & Kimura, K. New proposal of standard specimens for illite crystallinity measurement: its usefulness as paleo-geothermal indicator. *Bull. Geol. Surv. Japan* **54**, 239–250 (2003).
41. de Caritat, P., Hutcheon, I. & Walshe, J. L. Chlorite geothermometry: a review. *Clays Clay Miner.* **41**, 219–239 (1993).
42. Wallis, S. R. & Okudaira, T. Paired metamorphic belts of SW Japan: the geology of the Sanbagawa and Ryoke metamorphic belts and the median tectonic line. *The Geol Japan*, 101–124 (Geol. Soc. London, 2016).
43. Tomurtogoo, O. *Tectonic Map of Mongolia at the Scale of 1:1,000,000, and Tectonics of Mongolia (Brief Explanatory Notes to Tectonic Map of Mongolia at the scale of 1:1,000,000)* (Mineral Resources Authority of Mongolia, 2003).
44. Tsukada, K. et al. Geological setting of basaltic rocks in an accretionary complex, Khangai-Khentei Belt Mongolia. *Island Arc* **22**, 227–241 (2013).

Acknowledgements

Author contributions

H. T.: field research in Japan and Mongolia, sample processing, experiments, data processing, and draft writing. S. D.: field research in Mongolia, sample processing, experiments, and data processing. B. N.: field research in Japan and Mongolia, and sample processing. K. T.: research designing, field research in Japan, Mongolia, and Russia, sample processing, data processing, and draft writing.

Declarations

Competing interests

The authors declare no competing interests.

Additional information

Correspondence and requests for materials should be addressed to K.T.

Reprints and permissions information is available at www.nature.com/reprints.

Publisher's note Springer Nature remains neutral with regard to jurisdictional claims in published maps and institutional affiliations.